PCCP

COMMUNICATION

View Article Online
View Journal | View Issue

Cite this: *Phys. Chem. Chem. Phys.*, 2017, **19**, 14897

Received 11th April 2017,
Accepted 16th May 2017

DOI: 10.1039/c7cp02350b

rsc.li/pccp

First-principles study of adsorption–desorption kinetics of aqueous V^{2+}/V^{3+} redox species on graphite in a vanadium redox flow battery†

Zhen Jiang, [a] Konstantin Klyukin [a] and Vitaly Alexandrov*[ab]

Vanadium redox flow batteries (VRFBs) represent a promising solution to grid-scale energy storage, and understanding the reactivity of electrode materials is crucial for improving the power density of VRFBs. However, atomistic details about the interactions between vanadium ions and electrode surfaces in aqueous electrolytes are still lacking. Here, we examine the reactivity of the basal (0001) and edge ($11\bar{2}0$) graphite facets with water and aqueous V^{2+}/V^{3+} redox species at 300 K employing Car–Parrinello molecular dynamics (CPMD) coupled with metadynamics simulations. The results suggest that the edge surface is characterized by the formation of ketonic C=O functional groups due to complete water dissociation into the H/O/H configuration with surface O atoms serving as active sites for adsorption of V^{2+}/V^{3+} species. The formation of V–O bonds at the surface should significantly improve the kinetics of electron transfer at the edge sites, which is not the case for the basal surface, in agreement with the experimentally hypothesized mechanism.

All-vanadium redox flow batteries (VRFBs) are an attractive technology for large-scale grid energy storage from intermittent sources with a number of appealing properties such as rapid response times, long life span and low cross-contamination by crossover of vanadium ions across the membrane.[1–4] In a VRFB, the redox-active species (V^{2+}, V^{3+}, VO^{2+} and VO_2^{+}) are dissolved in an acid-based electrolyte, and during discharge V^{2+} is oxidized to V^{3+} while VO_2^{+} is reduced to VO^{2+} at the electrode, and these reactions are reversed during charging. One of the critical parameters that dictate the overall efficiency of VRFBs is power density. To develop VRFBs with higher power density, atomistic details about the electrochemical reactions at the electrolyte/electrode interfaces are warranted.[5]

In the past years, carbon-based electrodes such as graphite, graphene and carbon nanotubes have been widely used in various electrochemical applications including RFBs due to their relatively low cost, wide operating potential range and stability in concentrated acid-based electrolytes.[5–10] However, pristine carbon electrodes are often characterized by relatively low electrochemical activity and poor kinetic reversibility. In order to develop electrocatalysts with enhanced catalytic activity and thus higher power density, understanding the structure of electrolyte/electrode interfaces and the reactivity of carbon electrodes towards vanadium redox couples at the microscale is crucial.

Recently, a number of experimental investigations have been undertaken to understand the kinetics and mechanisms of V^{2+}/V^{3+} and VO^{2+}/VO_2^{+} redox transformations at the carbon electrodes.[11–16] However, the results are still rather contradictory regarding the overall mechanism, the rate limiting step and how various factors affect the redox kinetics. For instance, some studies suggested that the vanadium redox reactions at the carbon electrodes proceed *via* a "slow" outer-sphere mechanism instead of the "rapid" inner-sphere mechanism,[17] however, it is still unclear how this depends on the solution and electrode chemistry. Nevertheless, most of the studies agree to a strong dependence of these redox reactions on the composition of the electrode material.[5,14–16]

In a recent X-ray photoelectron spectroscopy based investigation[14] of the role of basal and edge carbon in the redox kinetics of V^{2+}/V^{3+} and VO^{2+}/VO_2^{+}, it was shown that the higher numbers of edge sites greatly enhance the reaction kinetics for both redox couples on heat-treated carbon, while the improved activity can be attributed to the presence of oxygen defects at the edge sites. Oxidation of carbon and the number of graphitic edge sites were observed to further go up as a result of the electrochemical oxidation of the graphite electrodes. After the treatment, different numbers of surface C–O, C=O and COOH functional groups were identified.[14–16]

[a] *Department of Chemical and Biomolecular Engineering, University of Nebraska-Lincoln, Lincoln, NE 68588, USA. E-mail: valexandrov2@unl.edu; Tel: +1 402 4725323*
[b] *Nebraska Center for Materials and Nanoscience, University of Nebraska-Lincoln, Lincoln, NE 68588, USA*

† Electronic supplementary information (ESI) available: Details on computational methodology (Section I) and *ab initio* metadynamics simulations including the choice of the number of Gaussian functions used to obtain free-energy profiles of the adsorption and desorption reaction (Section II). See DOI: 10.1039/c7cp02350b

It was also demonstrated that by varying the oxidation techniques, the number and types of surface oxygen functional groups can be tailored leading to an improved performance of VRFBs.[16]

The chemistry of vanadium species in aqueous electrolytes has been previously investigated in detail both experimentally and computationally with a particular emphasis on the precipitation reactions and thermal stability of vanadium electrolytes,[18–20] atomic structure of aqueous vanadium ions and their speciation with electrolyte species,[21–24] as well as interactions between vanadium ions and membranes.[4,25] However, so far very little attention has been paid to understanding the reactivity of carbon surfaces in the aqueous phase towards vanadium redox reactions and adsorption behavior of vanadium ions at the atomic level. Here, we examine the interaction between V^{2+}/V^{3+} half-cell reaction species and graphite basal and edge surfaces by combining static density-functional-theory (DFT) calculations with Car–Parrinello molecular dynamics (CPMD) simulations explicitly treating aqueous solution at 300 K.

Our DFT calculations of surface energies show that the $(11\bar{2}0)$ armchair edge is more stable than the $(10\bar{1}0)$ zigzag edge by 1.0 J m^{-2} (Table 1), and therefore we only compare the basal case with the armchair edge termination. Before considering adsorption of vanadium ions at the surfaces, we first analyze the interaction between water and both the basal and armchair edge surfaces. For the basal plane, we find that H_2O molecules prefer to interact with the basal plane of graphite in a molecular mode rather than to dissociate at the surface. In particular, the adsorption energy of a single H_2O is computed to be −3.3 kcal mol^{-1}, which is comparable to that previously calculated for the basal graphene (−2.8 kcal mol^{-1}).[26]

It was hypothesized in the experimental literature that the reactivity of the graphite basal surface towards vanadium redox reactions could be enhanced by introducing surface OH groups through the (electro)chemical treatment.[5,14] We consider different adsorption sites and find that OH adsorption atop the top (T) site is more stable than over hollow (H) or bridge (B) sites in static DFT calculations (Fig. 1(b)). The adsorption energy estimated as the energy difference between the adsorbed (atop the T site of graphite) and desorbed (in the middle of the vacuum gap) OH states is determined to be about 6.5 kcal mol^{-1}. However, in CPMD simulations of aqueous solution at 300 K we observe that the OH group is stable on the basal surface only if the nearest-neighbor carbon is protonated, and if the site is not protonated then OH will immediately leave the surface. In addition, we find in CPMD simulations that the presence of an aqueous vanadium ion in the vicinity of a surface OH group triggers the recombination of OH with a neighboring proton to form H_2O that leaves the surface.

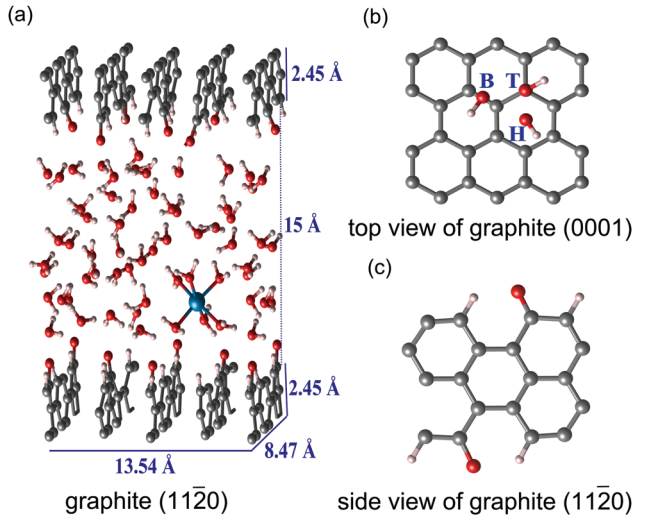

Fig. 1 Simulation cell used to model adsorption of V^{2+}/V^{3+} species in an aqueous phase (a), top view of the basal (0001) graphite surface with possible adsorption sites hollow (H), bridge (B) and top (T) (b), and side view of the edge $(11\bar{2}0)$ graphite surface with the most favorable H/O/H adsorption configuration of water (c).

In the case of the edge surface, we find that the armchair edge sites are so reactive that H_2O molecules completely dissociate into two H atoms and one O atom (H/O/H state) as shown in Fig. 1(c). Static DFT calculations show that this is indeed the most favorable hydroxylation state leading to 96.3 kcal mol^{-1} lower energy than the system with molecular water (Table 2). We observe that this hydroxylated surface is stable during CPMD simulations, whereas any intermediate cases (with varying numbers of surface H_2O, OH/O and H/O/H species) converge to the most stable H/O/H case over time. We should note that we were not able to obtain a full coverage of the edge surface by H/O/H species in our simulations since the used surface cell does not allow us to evenly distribute three H/O/H species. Overall, this result is in full agreement with a recent DFT study of water dissociation at the graphene edge sites[16,26] showing that the H/O/H state is more stable than H/OH by 55.4 kcal mol^{-1} (2.4 eV) in the dilute regime, while molecular H_2O adsorption is unstable. In addition, the presence of surface C═O groups on the edge graphite was observed in recent experimental studies.[14–16] Thus, our calculations demonstrate that OH groups are rather unstable on the basal plane of graphite, while on the armchair edge surfaces water should dissociate completely with the formation of ketonic C═O functional groups.

Knowing the atomic structure of the water/graphite interface, we next investigate the adsorption–desorption behavior of

Table 1 Calculated surface energies (in J m^{-2}) for the (0001) basal, $(11\bar{2}0)$ edge armchair and $(10\bar{1}0)$ edge zigzag surfaces of graphite

Surface	(0001)	$(11\bar{2}0)$	$(10\bar{2}0)$
This work	0.18	5.09	6.13
Other works	0.18[27,28]	4.60,[28] 5.33[29]	6.57,[28] 7.02[29]

Table 2 Adsorption energies (in kcal mol^{-1}) for molecular and dissociative modes of H_2O adsorption on the basal (0001) and edge $(11\bar{2}0)$ surfaces of graphite

Graphite	Molecular H_2O	OH/H	O/H/H
(0001)	−3.3	67.4	Unstable
$(11\bar{2}0)$	Unstable	−89.1	−96.3

Table 3 Adsorption energies from outer-sphere to inner-sphere adsorbed configurations (in kcal mol^{-1}) of aqueous V^{2+} and V^{3+} species for pristine and hydroxylated (0001) and (11$\bar{2}$0) graphite surfaces as computed in static DFT calculations

Surface	Pristine (0001)	Hydroxylated (0001)	Pristine (11$\bar{2}$0)	Hydroxylated (11$\bar{2}$0)
V^{2+}	5.3	24.0	−30.1	−8.3
V^{3+}	13.9	43.8	−44.7	−8.7

V^{2+} and V^{3+} in an aqueous phase over the basal and edge graphite surfaces. Since the basal plane is characterized by low reactivity towards water adsorption/dissociation, we compare the interaction of aqueous vanadium species for both pristine and hydroxylated surfaces of graphite.

Static DFT calculations of adsorption energies for aqueous vanadium ions (Table 3) reveal that for pristine graphite surfaces outer-sphere adsorption configurations are energetically preferred over inner-sphere complexes on the basal surface, while this is the opposite for the edge surface. Also, the most favorable inner-sphere adsorption complex of V^{3+} is more stable at the edge sites than that of V^{2+} by 14.6 kcal mol^{-1}. For the hydroxylated surfaces, we again observe the preference of outer-sphere over inner-sphere complexes for the basal plane and the opposite for the edge surface.

To investigate the adsorption–desorption kinetics of V^{2+} and V^{3+} in aqueous solution on the hydroxylated edge graphite, we perform CPMD-based metadynamics simulations to obtain free-energy barriers at 300 K. It is seen from the simulated free-energy profiles shown in Fig. 2 that the activation barriers for adsorption from the outer-sphere to inner-sphere complex are comparable for V^{2+} and V^{3+} species (16–17 kcal mol^{-1}). The barriers for desorption, however, are different being larger for V^{3+} (34.3 kcal mol^{-1}) than for V^{2+} (24.9 kcal mol^{-1}), which can

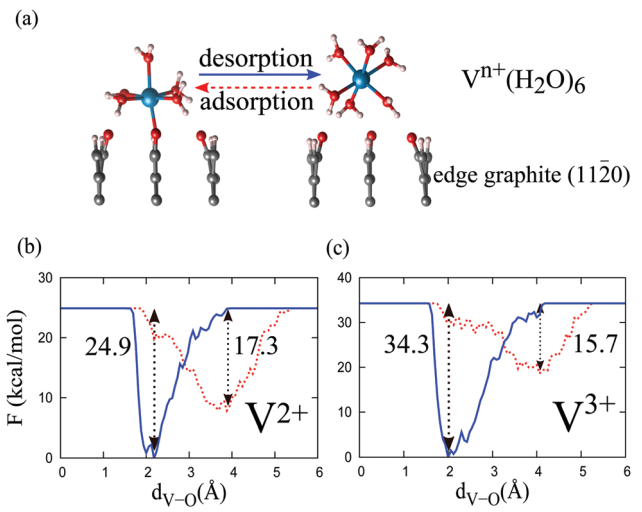

Fig. 2 Free-energy profiles for the adsorption–desorption processes between outer- and inner-sphere adsorption configurations of aqueous V^{2+} and V^{3+} species as computed by CPMD-based metadynamics. Only H_2O molecules from the first coordination sphere of V^{n+} are shown, while the rest H_2Os are removed for clarity.

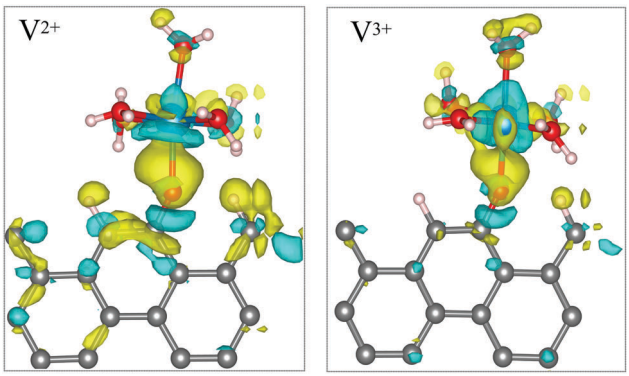

Fig. 3 Electron density difference maps (EDDM) of the inner-sphere adsorbed structure of aqueous V^{2+} and V^{3+} species on the edge graphite (11$\bar{2}$0) surface, where the yellow and green parts in the EDDM denote the increase and decrease of the electron density arising from the adsorption process, respectively.

be qualitatively explained by a stronger V^{3+}–O bond due to the larger electrostatic attraction between V^{3+} and the surface O atom in the inner-sphere adsorption configuration. We also point out that in an acidic environment of a VRFB aqueous electrolyte there should be a dynamic equilibrium between bare and protonated surface O atoms which will depend on the solution pH, however, we estimate that both aqueous V^{2+} and V^{3+} ions have larger driving forces to adsorb on a bare O site than that of a proton from H_3O^+.

It was previously shown experimentally that the presence of oxygen functional groups on the carbon surface should greatly promote the kinetics of V^{2+}/V^{3+} and VO^{2+}/VO_2^+ redox reactions, as well as improve the Coulombic, voltage and energy efficiencies of the whole VRFBs.[14–16] Our analysis of the projected density of states (PDOS) for the most favorable inner-sphere complexes at the O atoms of the edge surfaces indeed shows a significant hybridization between O 2p and V 3d states that should result in rapid electron transfer across the interface. In addition, a pronounced accumulation of electron density along the V–O bonds caused by adsorption of vanadium ions at the surface is clearly seen from the electron density difference maps (EDDM) shown in Fig. 3.

Conclusions

In conclusion, our calculations reveal that the basal surface of graphite should be rather inactive towards V^{2+}/V^{3+} redox reactions since inner-sphere vanadium complexes are less stable than outer-sphere complexes at the surface and thus electron transfer should primarily proceed through the outer-sphere adsorption configurations. On the other hand, the edge graphite surface is characterized by the formation of ketonic C═O surface groups due to its high reactivity towards water splitting into H/O/H species. These surface oxygen sites serve as active sites for adsorption of aqueous vanadium ions at the edges and should facilitate rapid electron transfer through the interface, in full agreement with an experimentally

hypothesized mechanism of the redox reaction. Our calculations also suggest that desorption of tightly bound V^{3+} species from the C═O groups of the edges might be the rate limiting step in the overall redox reaction during battery discharge.

Computational details

Calculations were carried out within the plane-wave density-functional-theory (DFT) framework as implemented in the NWChem code.[30] The exchange and correlation energies were calculated using the Perdew–Burke–Ernzerhof (PBE) functional within the generalized gradient approximation (GGA).[31] The PBE functional was corrected for van der Waals interactions using the Grimme approach (PBE-D3 with BJ damping).[32] The norm-conserving Troullier–Martins pseudopotentials[33] were used for vanadium and Hamann pseudopotentials[34,35] were used for oxygen, carbon and hydrogen. The kinetic cutoff energies of 100 and 200 Ry were applied to expand the Kohn–Sham electronic wave functions and charge density, respectively. The (0001), $(11\bar{2}0)$ and $(10\bar{1}0)$ graphite surfaces were modelled as periodic slabs comprised of two, five and six atomic layers with a vacuum gap of 15 Å, while the surface dimensions were 9.78×9.78 (4×4 unit cell), 13.54×8.47 (2×2 unit cell) and 13.54×7.34 Å^2 (2×3 unit cell), respectively. The lattice parameters of graphite were first optimized using the Bernal structure unit cell[36] resulting in $a = b = 2.45$ Å and $c = 6.77$ Å. Car–Parrinello molecular dynamics (CPMD)[37] simulations at the Γ-point were performed with one vanadium ion and 41 H_2O molecules for the (0001) surface and 49 H_2O molecules for the $(11\bar{2}0)$ surface to provide a water density of 1 g cm^{-3}. The Nose–Hoover thermostat[38,39] was employed to maintain the system temperature at 300 K. The aqueous systems were initially pre-equilibrated using a QM/MM potential[40] for 20 ps followed by additional CPMD equilibration for 5 ps. Further computational details including parameters for CPMD metadynamics simulations are provided in the ESI.†

Acknowledgements

The authors thank Dr Eric Bylaska (Pacific Northwest National Laboratory) for his help with the NWChem code. This research used resources of the National Energy Research Scientific Computing Center, a DOE Office of Science User Facility supported by the Office of Science of the U.S. Department of Energy under Contract No. DE-AC02-05CH11231. Also, we would like to acknowledge the Holland Computing Center at the University of Nebraska-Lincoln for providing computational resources. V. A. is grateful for financial support from the Layman seed grant and the startup package provided by the University of Nebraska-Lincoln.

References

1 Z. Yang, J. Zhang, M. C. Kintner-Meyer, X. Lu, D. Choi, J. P. Lemmon and J. Liu, *Chem. Rev.*, 2011, **111**, 3577–3613.
2 A. Z. Weber, M. M. Mench, J. P. Meyers, P. N. Ross, J. T. Gostick and Q. Liu, *J. Appl. Electrochem.*, 2011, **41**, 1137.
3 A. Parasuraman, T. M. Lim, C. Menictas and M. Skyllas-Kazacos, *Electrochim. Acta*, 2013, **101**, 27–40.
4 D. Chen and M. A. Hickner, *Phys. Chem. Chem. Phys.*, 2013, **15**, 11299–11305.
5 K. J. Kim, M.-S. Park, Y.-J. Kim, J. H. Kim, S. X. Dou and M. Skyllas-Kazacos, *J. Mater. Chem. A*, 2015, **3**, 16913–16933.
6 M. Park, J. Ryu and J. Cho, *Chem. – Asian J.*, 2015, **10**, 2096–2110.
7 S. Zhong and M. Skyllas-Kazacos, *J. Power Sources*, 1992, **39**, 1–9.
8 X. Liu and L. Dai, *Nat. Rev. Mater.*, 2016, **1**, 16064.
9 S. Ayissi, K. Pilotas, H. Qin, L. Yang and P. A. Charpentier, *Phys. Chem. Chem. Phys.*, 2016, **18**, 29208–29217.
10 M. Park, J. Ryu, W. Wang and J. Cho, *Nat. Rev. Mater.*, 2016, **2**, 16080.
11 G. Oriji, Y. Katayama and T. Miura, *J. Power Sources*, 2005, **139**, 321–324.
12 D. Aaron, C.-N. Sun, M. Bright, A. B. Papandrew, M. M. Mench and T. A. Zawodzinski, *ECS Electrochem. Lett.*, 2013, **2**, A29–A31.
13 A. Bourke, N. Quill, R. P. Lynch and D. N. Buckley, *ECS Trans.*, 2014, **61**, 15–26.
14 N. Pour, D. G. Kwabi, T. Carney, R. M. Darling, M. L. Perry and Y. Shao-Horn, *J. Phys. Chem. C*, 2015, **119**, 5311–5318.
15 H. Fink, J. Friedl and U. Stimming, *J. Phys. Chem. C*, 2016, **120**, 15893–15901.
16 L. Estevez, D. Reed, Z. Nie, A. M. Schwarz, M. I. Nandasiri, J. P. Kizewski, W. Wang, E. Thomsen, J. Liu and J.-G. Zhang, *et al.*, *ChemSusChem*, 2016, **9**, 1455–1461.
17 T. Yamamura, N. Watanabe, T. Yano and Y. Shiokawa, *J. Electrochem. Soc.*, 2005, **152**, A830–A836.
18 L. Li, S. Kim, W. Wang, M. Vijayakumar, Z. Nie, B. Chen, J. Zhang, G. Xia, J. Hu and G. Graff, *et al.*, *Adv. Energy Mater.*, 2011, **1**, 394–400.
19 J. Noack, N. Roznyatovskaya, T. Herr and P. Fischer, *Angew. Chem., Int. Ed.*, 2015, **54**, 9776–9809.
20 M. Skyllas-Kazacos, L. Cao, M. Kazacos, N. Kausar and A. Mousa, *ChemSusChem*, 2016, **9**, 1521–1543.
21 M. Kim, S. Vijayakumar, W. Wang, J. Zhang, B. Chen, Z. Nie, F. Chen, J. Hu, L. Li and Z. Yang, *Phys. Chem. Chem. Phys.*, 2011, **13**, 18186–18193.
22 M. Vijayakumar, L. Li, Z. Nie, Z. Yang and J. Hu, *Phys. Chem. Chem. Phys.*, 2012, **14**, 10233–10242.
23 M. Bon, T. Laino, A. Curioni and M. Parrinello, *J. Phys. Chem. C*, 2016, **120**, 10791–10798.
24 Z. Jiang, K. Klyukin and V. Alexandrov, *J. Chem. Phys.*, 2016, **145**, 114303.
25 D. Chen, M. A. Hickner, E. Agar and E. C. Kumbur, *Electrochem. Commun.*, 2013, **26**, 37–49.
26 G. Levita, P. Restuccia and M. Righi, *Carbon*, 2016, **107**, 878–884.
27 R. E. Ambrusi, S. G. Garca and M. E. Pronsato, *Appl. Surf. Sci.*, 2015, **324**, 710–717.
28 S. Thinius, M. M. Islam and T. Bredow, *Surf. Sci.*, 2016, **649**, 60–65.

29 A. Incze, A. Pasturel and C. Chatillon, *Appl. Surf. Sci.*, 2001, **177**, 221–225.
30 M. Valiev, E. J. Bylaska, N. Govind, K. Kowalski, T. P. Straatsma, H. J. Van Dam, D. Wang, J. Nieplocha, E. Apra and T. L. Windus, *et al.*, *Comput. Phys. Commun.*, 2010, **181**, 1477–1489.
31 J. P. Perdew, K. Burke and M. Ernzerhof, *Phys. Rev. Lett.*, 1996, **77**, 3865.
32 S. Grimme, S. Ehrlich and L. Goerigk, *J. Comput. Chem.*, 2011, **32**, 1456–1465.
33 N. Troullier and J. L. Martins, *Phys. Rev. B: Condens. Matter Mater. Phys.*, 1991, **43**, 1993.
34 D. Hamann, M. Schlüter and C. Chiang, *Phys. Rev. Lett.*, 1979, **43**, 1494.
35 D. Hamann, *Phys. Rev. B: Condens. Matter Mater. Phys.*, 1989, **40**, 2980.
36 J. Bernal, *Proc. R. Soc. London, Ser. A*, 1924, **106**, 749–773.
37 R. Car and M. Parrinello, *Phys. Rev. Lett.*, 1985, **55**, 2471.
38 S. Nosé, *Mol. Phys.*, 1984, **52**, 255–268.
39 W. G. Hoover, *Phys. Rev. B: Condens. Matter Mater. Phys.*, 1985, **31**, 1695.
40 E. Cauët, S. Bogatko, J. H. Weare, J. L. Fulton, G. K. Schenter and E. J. Bylaska, *J. Chem. Phys.*, 2010, **132**, 194502.